11th Australasian Fluid Mechanics Conference
University of Tasmania, Hobart, Australia
14-18 December 1992

A NUMERICAL STUDY OF COMPLEX CAVITY FLOWS VIA THE NAVIER-STOKES EQUATIONS

C.A. ATWOOD and W.R. VAN DALSEM

NASA Ames Research Center
Moffett Field, CA 94035-1000, USA

Abstract

Numerical solutions for the flow fields about several cavity configurations have been computed using the Reynolds-averaged Navier-Stokes equations. Comparisons between numerical and experimental results are made in two-dimensions for free shear layers and a rectangular cavity, and in three-dimensions for the transonic aero-window problem of the Stratospheric Observatory For Infrared Astronomy (SOFIA). Results show that dominant acoustic frequencies and magnitudes of the self-excited resonant cavity flows compare well with experiment. In addition, solution sensitivity to artificial dissipation and grid resolution levels are determined. Furthermore, optical path distortion due to the flow field is modelled geometrically and is found to match the experimental trend.

Introduction

The design of a safe and effective airborne observatory provides motivation for this study of self-excited open cavities. The SOFIA airborne observatory will be a three meter class Cassegrain telescope which utilizes a Boeing 747SP as an observation platform. An artist's concept of the observatory, which is currently a cooperative effort between the United States' NASA and Germany's DARA, is shown in Fig. 1. Risk of injury to the crew or damage to the platform is presently being reduced through experimental and computational fluid dynamical (CFD) analyses. This paper summarizes the analysis methodology developed for use in the SOFIA design, of which a detailed outline can be found in Atwood and Van Dalsem (1992).

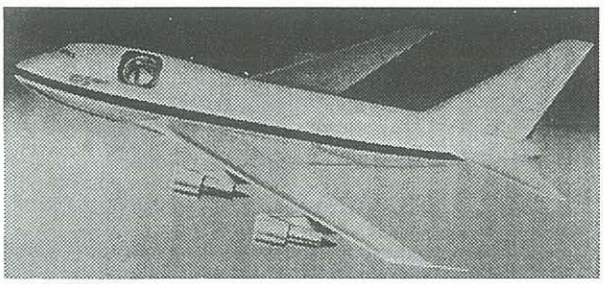

Fig. 1: Artist's concept of the SOFIA configuration

Although extensive experimental and numerical studies have been conducted on the driven cavity problem, the objective of this effort is to assess the accuracy of a general and efficient numerical method. Towards this goal, the following sections compare numerical solutions against analytical and experimental results for two-dimensional shear layers and a rectangular cavity flow field. Additional validation is provided by comparison of computed SOFIA flows with the experimental data of Rose and Cooley (1990).

Numerical Method

General solution of these cavity problems were computed using models for the fluid field, the effect of turbulence, and the optical distortion. The fluid field was computed via the Navier-Stokes equations using the diagonal scheme of Pulliam and Chaussee (1981) implemented in the overset grid framework of Benek, Buning, and Steger (1985). The equations were integrated through Euler implicit time marching and second-order spatial differencing with viscous impermeable wall conditions specified as no-slip, zero normal pressure gradient, and adiabatic. Information transfer across overset mesh boundaries was implemented using trilinear interpolation of the dependent variable vector, $Q = [\rho, \rho u, \rho v, \rho w, e]^T$.

The effect of turbulence was modelled using the method of Baldwin and Lomax (1978) modified with a variable F_{max} cutoff and a shear layer model. The eddy viscosity in the shear layer was computed using the outer region portion of the Baldwin-Lomax model, with σ_0 set equal to 11.0 according to experimental, though quite variable, values as compiled by Birch and Eggers (1972).

Finally, since the speed of light through a gas is a function of the density field, image distortion can be computed using the density history of the shear layer. This effort used geometrical optics in conjunction with the Gladstone-Dale relationship to compute the fluctuating optical path difference, $< OPD(x)' >$, from which image distortion was determined.

Results

Free Shear Layer

Numerical experiments were performed using a two-dimensional shear layer to determine sensitivities of mean and time-varying quantities to changes in time step size, fourth-order dissipation levels, and grid refinement. In addition, the algebraic turbulent shear layer model was partially validated through comparison with similarity solutions and experimental data.

*Research Scientist, MCAT Institute
†Research Scientist and Group Leader

The computational domain for this case is shown to scale in Fig. 2a, where inviscid channel side walls and characteristic inflow and outflow boundary conditions were used. The boundary layers on the splitter plate and the shear layer were fully turbulent with a Reynolds number based on the mean velocity of the streams and the length of the splitter plate given as 6.7×10^5.

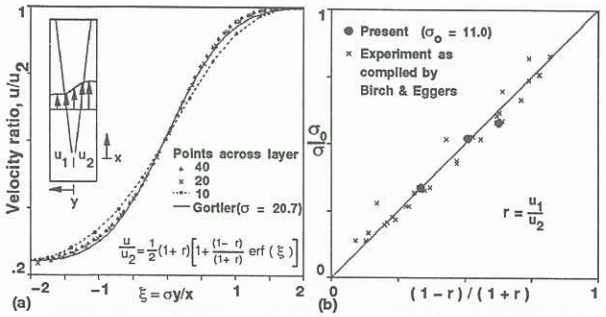

Fig. 2: (a) Velocity profiles of differing grid resolution compared to similarity and (b) Variation of spread rate with velocity ratio

The results for three grid refinement levels are also shown in Fig. 2a along with Görtler's similarity solution, where the velocity profiles were taken more than a thousand momentum thicknesses downstream of the trailing edge of the plate. The solution can be seen to become grid dependent when fewer than than 20 points span the layer. Eddy viscosity was observed to grow linearly in accordance with the Clauser formulation, while the solution was insensitive to fourth-order dissipation levels within the range 0.01 to 0.05. The Mach ratio for this case was 0.2/0.8 with $\sigma = 20.7$, where spreading parameter σ originates from the similarity solution shown in Fig. 2a. The spread rate is inversely related to σ, denoted σ_0 when the velocity of one of the streams is zero.

Figure 2b compares the variation of spread rate with velocity ratio, and demonstrates that computed spreading rates are within the bounds of the experimental data.

Two-Dimensional Cavity

The objective of the two-dimensional cavity computation was to demonstrate the prediction of self-induced cavity resonance. Validation data is provided by comparison against Rossiter's (1964) experiment. Sensitivity of the solution to topology, second-order dissipation, and turbulence model effects were determined.

The test conditions, specified to match experiment, were $M_\infty = 0.9$, $Re_L = 1.47 \times 10^6$, $L = 8\ in.$, and a cavity length by depth, L/D, of 2. Characteristic inflow and outflow conditions were specified along with a step size of $\Delta t = 1.97 \mu s$.

Inspection of the computed cavity pressure history, shown in Fig. 3a, confirms the idealized feedback mechanism identified by Rossiter. Briefly, the cycle begins with the propagation of an acoustic wave from the aft wall of the cavity to the forward bulkhead. Wave reflection from the forward wall causes the shear layer to bow outwards, shedding vorticity. The deflected shear layer convects downstream and induces another cycle. The frequencies at which this feedback is reinforced is determined by ambient temperature and Mach number.

In the frequency domain, comparison of Rossiter's data to present results indicate agreement in frequency at the

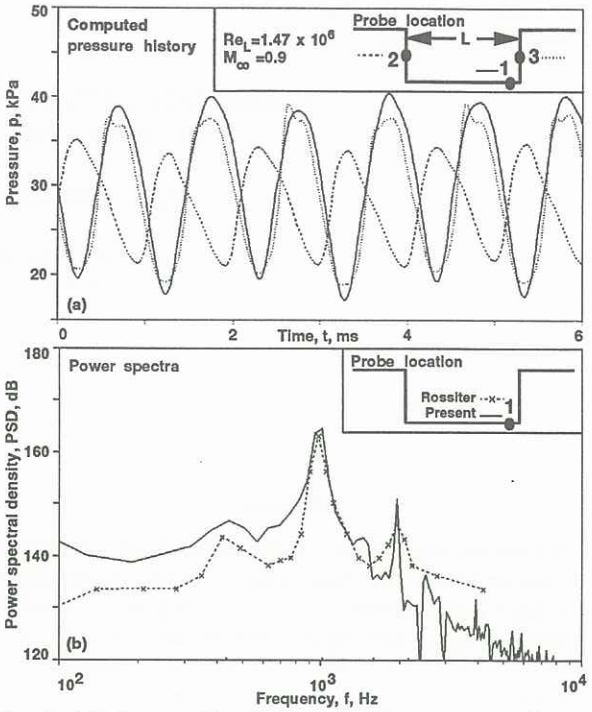

Fig. 3: (a) Pressure histories and (b) Power spectra of rectangular cavity

peak magnitudes, as shown in Fig. 3b. Magnitudes are higher for the present case by about 2 dB, which can be explained from dimensionality arguments. The solution was also found to be insensitive to second-order dissipation levels within the range 0.3 to 0.5.

Numerically and experimentally determined mean and root mean square pressures along the cavity walls are shown in Fig. 4. The trends appear reasonable given the flow complexity, the difference in spatial dimensions, and turbulence modelling assumptions. Finally, the vertical knife edge schlieren images of Fig. 5 show the qualitative agreement between computed and observed radiation patterns.

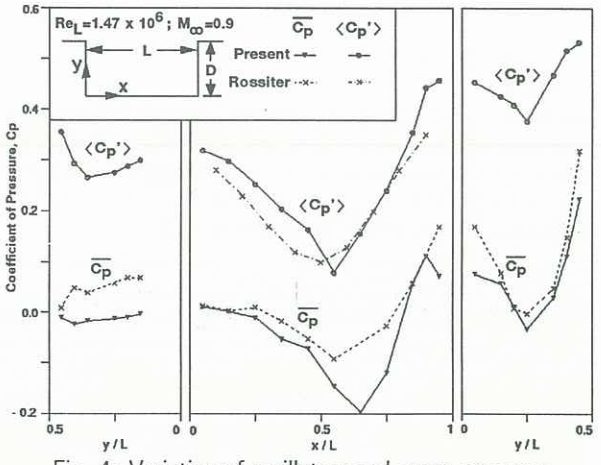

Fig. 4: Variation of oscillatory and mean pressures

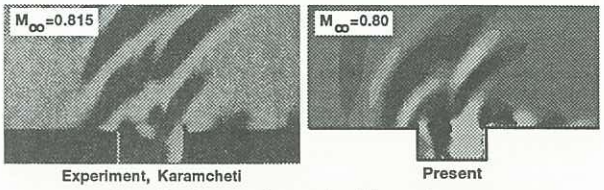

Fig. 5: Comparison of schlieren images

Configuration 25

This simulation was implemented in order to demonstrate the capture of self-excited cavity resonance in three-dimensions. The flow conditions were initialized from a clean steady case, using test conditions which matched experiment, $M_\infty = 0.85$, $Re_L = 4.2 \times 10^6$, $\alpha = 2.5°$, and $L = 12.6\ in.$. The stability-limited time step size was $\Delta t = 3.53\mu s$, corresponding to a Courant number, ν, of one in the streamwise direction within the shear layer, and a $\nu_{max} \approx 500$.

Figure 6 shows reasonable prediction of dominant tone frequencies, with the computed dominant tone within 3 dB of experiment. However, the magnitudes of the higher modes were much lower than found experimentally due to grid coarseness. Analysis of the spectra from the resonating cavity cases has shown that 40 points are required to accurately propagate a travelling wave in the cavity.

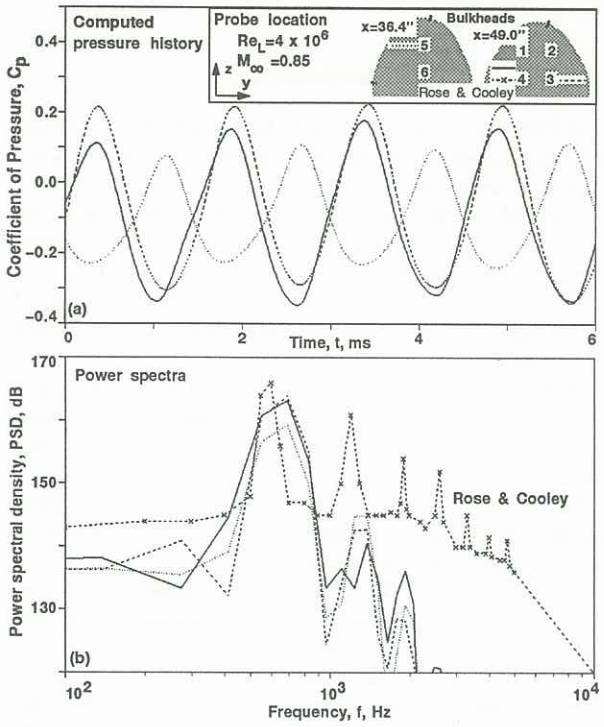

Fig. 6: Configuration 25: (a) pressure history and (b) power spectra

Although numerical damping of higher frequencies can be expected, the bulk of the energy is contained in the low frequency modes, as shown in Fig. 7. The computed sound pressure levels for the resonating and quieted geometries are in reasonable agreement with experiment.

Configuration 100

The flow about configuration 100 was implemented in order to determine if the same level of quieting would be predicted numerically as was found experimentally. Previous investigations of cavity noise suppression have shown aft ramp treatments to be effective by allowing a stable shear layer reattachment site. For the SOFIA experiment, this type of geometry treatment was found to be quieter than the untreated configuration 25 case by over 30 dB, as shown in Fig. 7. Using flow conditions again initialized from the clean case, the stability-limited time step size used was $\Delta t = 7.06\mu s$.

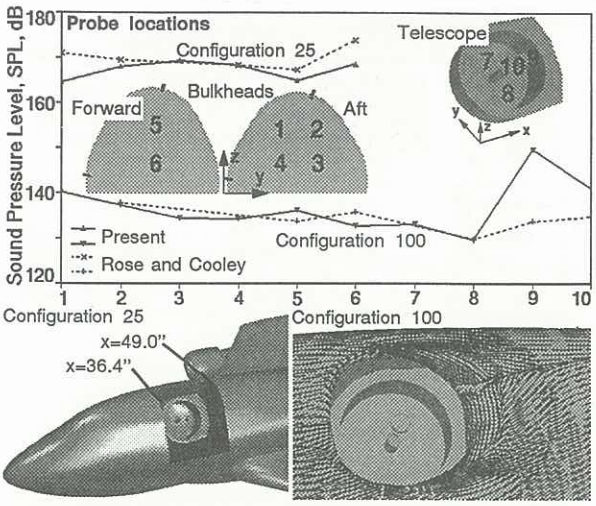

Fig. 7: Comparison of sound pressure levels

Figure 7 also shows the position of the telescope in the aircraft and the aft ramp treatment modelled for this case along with the computed surface flow pattern. Figure 9 compares the mean experimental and computational shear layer Mach profiles, indicating reasonable agreement for growth rates. The discrepancy in the profile shapes as the shear layer approaches the ramp may be in part due to an overly high value specified for σ_0, probe position uncertainty, or geometry modifications to allow for the probe mechanism. Figure 8 shows the general agreement of the broadband spectra, however the spectra levels were again seen to drop more rapidly with frequency for the numerical as compared to the experimental results. Computed results at the secondary mirror showed a low frequency component which was not found experimentally. This discrepancy was manifested as a difference in sound pressure levels at probe location 9, as shown in Fig. 7.

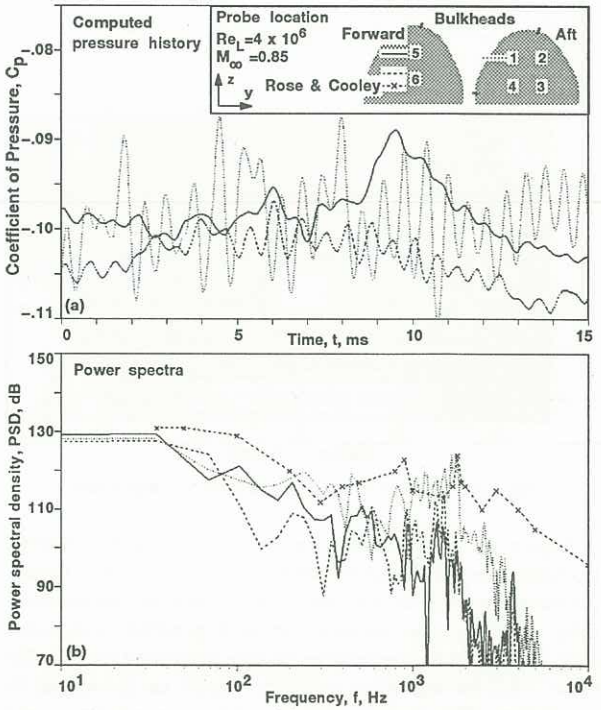

Fig. 8: Configuration 100: (a) pressure history and (b) power spectra

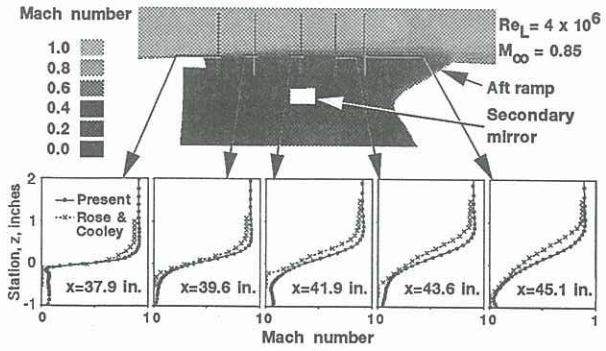

Fig. 9: Mean Mach profiles for configuration 100

Aero-optics

The optics code was applied to the density field obtained from configuration 100 at the cross flow center of the aperture. Ten rays were propagated through 110 density fields in time intervals of $\Delta t = 70.6\mu s$, sufficient for several shear layer perturbation cycles to occur. Computed fluctuating optical path differences, $< OPD' >$, are compared to experiment and previous analysis of Bogdanoff (1984) in Fig. 10. Two computed results are shown, one for the optical integration paths originating immediately below the shear layer ($r_0 = -0.7\ in.$), and the other for rays initialized below the secondary mirror ($r_0 = -3.7\ in.$). All computed integration paths terminate at $r_f = 2.3\ in.$ Shear layer aerodynamic measurements of Rose and Cooley (1990) were used to determine distortion for the experimental data shown in Fig. 10 while the analytic result assumes an index-matched shear layer with a sinusoidal n profile.

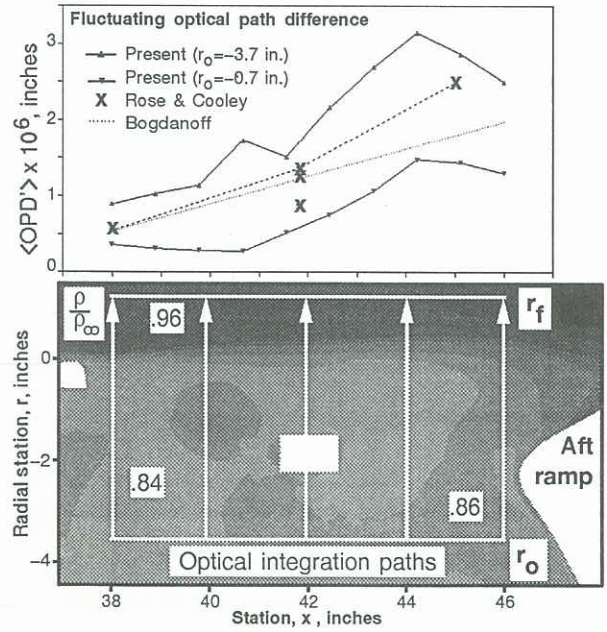

Fig. 10: Optical model and wavefront distortion

Figure 10 shows that the distortion model applied through the shear layer alone ($r_0 = -0.7\ in.$) underpredicts the data determined analytically and experimentally. However, the computed trend is generally consistent with the data. Comparison of the computed results for $r_0 = -0.7\ in.$ and $r_0 = -3.7\ in.$ shows an increment in $< OPD' >$. This distortion increment appears to be caused by a jet of fluid resulting from the impingement of the shear layer on the aft ramp.

Conclusions

The work presented here is the initial effort towards development of a design and analysis tool for use throughout the SOFIA project life. Thus far, this investigation has demonstrated that self-induced cavity resonance can be accurately captured for complex geometries modelled using an overset mesh topology. Generally, sound pressure levels agree to within 4% while shear layer profiles and resonant behaviour are consistent with previous analytic and experimental work. Topology treatment has allowed the simple specification of turbulent wall and shear layer regions as well as providing a means of isolating the unsteady flow region. Finally, the geometrical aero-optics model shows proper trends, but the distortion magnitude is underpredicted.

A continuing effort is being undertaken to incorporate a higher-order turbulence model as well as further validation and improvement of the aero-optical model.

References

ATWOOD, C.A. and VAN DALSEM, W.R., "Flowfield Simulation about the SOFIA Airborne Observatory," AIAA-92-0656, Jan. 1992.

BALDWIN, B.S. and LOMAX, H., "Thin-Layer Approximation and Algebraic Model for Separated Turbulent Flows," AIAA-78-257, Jan. 1978.

BENEK, J.A., BUNING, P.G., and STEGER, J.L.,"A 3-D Chimera Grid Embedding Technique," AIAA-85-1523, July 1985.

BIRCH, S.F. and EGGERS, J.M.,"A Critical Review of the Experimental Data for Developed Free Turbulent Shear Layers," *Free Turbulent Shear Flows,* NASA SP-321, July 1972.

BOGDANOFF, D.W., "The Optical Quality of Shear Layers: Prediction and Improvement Thereof," *AIAA J.*, Vol. 22, Jan. 1984, pp. 58-64.

KARAMCHETI, K,,"Acoustic Radiation from Two-Dimensional Rectangular Cutouts in Aerodynamic Surfaces," NACA TN-3487, 1955.

PULLIAM, T.H. and CHAUSSEE, D.S.,"A Diagonal Form of an Implicit Approximate-Factorization Algorithm," *J. Comp. Phys.*, Vol. 39, Feb. 1981, pp. 347-363.

ROSE, W.C. and COOLEY, J.M.,"SOFIA Wind Tunnel Data Analysis and Implications for the Full-Scale Aircraft," Rose Eng. and Research, Inc., Dec. 1990.

ROSSITER, J.E., "Wind-Tunnel Experiments on the Flow Over Rectangular Cavities at Subsonic and Transonic Speeds," Royal Aircraft Establishment Reports and Memoranda No. 3438, Oct. 1964.